Proceedings of the 22th National and 11th International ISHMT-ASME Heat and Mass Transfer Conference December 28-31, 2013, IIT Kharagpur, India

HMTC1300616

ENHANCED PERFORMANCE OF A NOVEL FUZZY CARBON FIBER HEAT EXCHANGER WITH CARBON NANOTUBES

S. I. Kundalwal
Dept. of Mechanical Engineering
Indian Institute of Technology
Kharagpur (WB)-721302, India
sikundalwal@iitkgp.ac.in

R. Suresh Kumar
Dept. of Mechanical Engineering
Indian Institute of Technology
Kharagpur (WB)-721302, India
rsureshiitkgp@mech.iitkgp.ernet.in

M. C. Ray
Dept. of Mechanical Engineering
Indian Institute of Technology
Kharagpur (WB)-721302, India
mcray@mech.iitkgp.ernet.in

ABSTRACT

A new fuzzy carbon fiber heat exchanger (FFHE) with carbon nanotubes (CNTs) is proposed in the present study. A novel constructional feature of the FFHE is that the uniformly spaced CNTs are radially grown on the outer circumferential surface of the hollow cylindrical carbon fiber (HCF). The effective thermal conductivities of a novel FFHE have been estimated by employing the method of cells (MOC) approach and the effective medium (EM) approach. The CNTs being radially grown on the outer circumferential surface of the HCF with their axes normal to this surface, significantly improve the transverse effective thermal conductivities of the FFHE over those of the bare HCF (i.e., without CNTs) heat exchanger e.g., almost 293% improvement occurs in the transverse effective thermal conductivities of the FFHE in the presence of only 9.93% of CNTs in the FFHE when the value of temperature is 400 K. It is also revealed that the CNT/ polymer matrix interfacial thermal resistance does not affect the effective thermal conductivities of the FFHE.

LIST OF ABBREVIATIONS

AF	Alignment Factor
CNT	Carbon Nanotube
EM	Effective Medium
FFHE	Fuzzy Carbon Fiber Heat Exchanger
HCF	Hollow Cylindrical Carbon Fiber
MOC	Method of Cells
PMNC	Polymer Matrix Nanocomposite
RUC	Repeating Unit Cell
SEM	Scanning Electron Microscopy

NOMENCLATURE

a_k	Kaptiza radius (m)
b	Width of the RUC (m)
b_γ	Width of the subcell (m)
d	Outer diameter of the HCF in the FFHE (m)
d_o	Outer diameter of the FFHE or the bare HCF (without CNTs) heat exchanger (m)
d_i	Inner diameter of the FFHE or the bare HCF (without CNTs) heat exchanger (m)
d_n	Diameter of the CNT (m)
h	Height of the RUC (m)
h_β	Height of the subcell (m)
K_i	Effective thermal conductivities of the FFHE (W/mK)
K^f	Thermal conductivity of the HCF (W/mK)
K^n	Thermal conductivity of the CNT (W/mK)
K_i^{nc}	Effective thermal conductivities of the unwound lamina of the PMNC (W/mK)
K^p	Thermal conductivity of the polymer (W/mK)
K_i^{PMNC}	Effective thermal conductivities of the PMNC (W/mK)
$K_i^{(\beta\gamma)}$	Thermal conductivity of the βγ-th subcell (W/mK)
L	Length of the FFHE (m)
L_n	Length of the CNT (m)
$(N_{CNT})_{max}$	Maximum number of radially grown aligned CNTs on the outer circumferential surface of the HCF
q_i	Heat flux in the unwound PMNC (W/m^2)
$\bar{q}_i^{(\beta\gamma)}$	Average heat flux in the βγ-th subcell (W/m^2)
R_k	Interfacial thermal resistance between the CNT and the polymer (m^2K/W)
T	Temperature (K)
[T]	Transformation matrix
V	Volume of the FFHE (m^3)
$V_{\beta\gamma}$	Volume of the βγ-th subcell (m^3)
$(V_{CNT})_{max}$	Maximum volume fraction of the CNTs in the FFHE
v_f	Volume fraction of the HCF in the FFHE
v_n	Volume fraction of the CNTs in the PMNC
v_p	Volume fraction of the polymer in the PMNC
v_{PMNC}	Volume fraction of the PMNC in the FFHE

INTRODUCTION

The identification of CNTs [1] has stimulated a great deal of research concerning the prediction of their remarkable mechanical and thermal properties. Many research investigations revealed that the axial Young's modulus of single-walled CNTs is in the terapascal range [2–4] and the thermal conductivity of single-walled CNTs greater than that of diamond and multi-walled CNTs [5–8]. In order to exploit the exceptional thermal conductivities of CNTs, extensive research is being carried out for developing the CNT-reinforced composites. For example, Choi *et al.* [9] produced nanotube-in-oil suspensions in a two-step process and measured their effective thermal conductivity. They found that the measured thermal conductivity is greater than theoretical predictions and is nonlinear with the CNT loadings. Biercuk *et al.* [10] fabricated CNT-reinforced composites and observed thermal conductivity enhancement greater than 125% at 1 wt% CNT loading. Guthy *et al.* [11] fabricated single-walled CNT/PMMA composites by employing the coagulation method with 6% CNT loading and found 240% enhancement in the thermal conductivity of single-walled CNT/PMMA composites. Nan *et al.* [12] found remarkable enhancement in the effective thermal conductivity of nanocomposites with the dispersion of a quite small amount of CNTs. The degree of enhancement of the thermal conductivity of nanocomposites varies substantially with CNT type, dispersion quality and CNT/polymer interfacial thermal resistance. The CNT/polymer interfacial thermal resistance may arise from the

mechanical/chemical bonding at the CNT/polymer interface and the thermal expansion mismatch. The interfacial thermal resistance is also known as the Kaptiza resistance. Wilson *et al.* [13] reported that the magnitude of interfacial thermal resistance between nanoparticles and different matrices ranges from 0.77×10^{-8} m^2K/W to 20×10^{-8} m^2K/W. The CNT/matrix interfacial thermal resistance reported by Huxtable *et al.* [14] is about 8.3×10^{-8} m^2K/W. Incorporating such CNT/matrix interfacial thermal resistance, Nan *et al.* [15] estimated the effective thermal conductivity of CNT-reinforced composite by employing the effective medium (EM) approach and predicted that the large value of the CNT/matrix interfacial thermal resistance causes significant degradation in the value of effective thermal conductivity. Subsequently, the effective thermal conductivities of nanocomposites are computed by several researchers [16–19] incorporating the CNT/matrix interfacial thermal resistance.

Further research on improving the out-of-plane multifunctional properties of the composites and the better use of short CNTs led to the growth of short CNTs on the surfaces of the advanced fibers [20–22]. Veedu *et al.* [23] demonstrated that the remarkable improvements in the multifunctional properties of the laminated composite can be obtained by growing multi-walled CNTs on the circumferential surfaces of the fibers. Their test results suggest that the presence of CNTs in the transverse (i.e., thickness) direction of the composite enhances the effective thermal conductivity up to 51% compared to that of the base composite. Electrophoresis technique has been utilized for the selective deposition of multi- and single-walled CNTs on the circumferential surfaces of the carbon fibers by Bekyarova *et al.* [24]. For the single-walled CNT/carbon fiber reinforced composites they demonstrated ~30% enhancement in the interlaminar shear strength and 2–fold improvement of the out-of-plane electrical conductivity as compared to that of the composite without CNTs. Multifunctional properties of the hybrid composite comprised of aligned CNTs grown *in situ* on the woven fibers and a thermoset polymer matrix have been characterized by Yamamoto *et al.* [25] and found that the loading of 2.2% CNTs in the hybrid composite enhances its effective thermal conductivity by two times over that of the base composite. Chen *et al.* [26] augmented the carbon/carbon composite by growing CNTs on the circumferential surface of the carbon fiber. The thermal conductivity of this composite becomes greater than that of the composite without CNTs. Fibers coated with radially grown CNTs on their circumferential surfaces are being called as “fuzzy fibers” [25, 27–29].

In the areas of high heat buildup such as carbon fiber heat exchangers, electric boards, engines and aerodynamically heated sections heat dissipation needs to be improved by the addition of thermal management advanced CNT-reinforced layers [27]. Hollow cylindrical carbon fiber (HCF) heat exchanger is an important element in many technological applications. Application of the CNT-reinforced polymer matrix layer on the outer circumferential surface of the HCF may enhance the heat dissipation across the thickness of the HCF heat exchanger. Unlike external metal layer that adds weight, the CNT-reinforced polymer matrix layer can enhance multifunctional properties of the HCF heat exchanger with minimum weight. Such HCF heat exchanger coated with the CNT-reinforced polymer matrix layer may be called as fuzzy carbon fiber heat exchanger (FFHE). However, the effective thermal conductivities of such a novel FFHE have not yet been reported. In this study, authors intend to estimate the thermal conductivities of the proposed FFHE and investigate the effect of the CNT/polymer matrix interfacial thermal resistance on the effective thermal conductivities of the FFHE.

ARCHITECTURE OF A NOVEL FFHE

The schematic diagram illustrated in Fig. 1 represents a novel FFHE being studied here. A novel constructional feature of the FFHE is that CNTs are radially grown on the outer circumferential surface of the HCF while they are uniformly spaced on the outer circumferential surface of the HCF. The

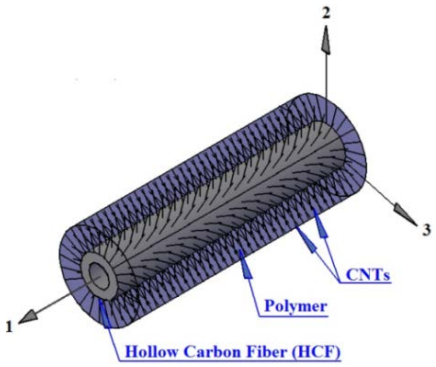

Figure 1. SCHEMATIC DIAGRAM OF A NOVEL FFHE

radially grown CNTs eventually reinforce the polymer matrix surrounding the HCF along the transverse direction to the length of the HCF. Thus the combination of the HCF with the CNTs and the polymer matrix can be viewed as a circular cylindrical composite FFHE in which the HCF is embedded in the CNT-reinforced polymer matrix nanocomposite (PMNC). Cross sections of such FFHE are schematically demonstrated in Fig. 2.

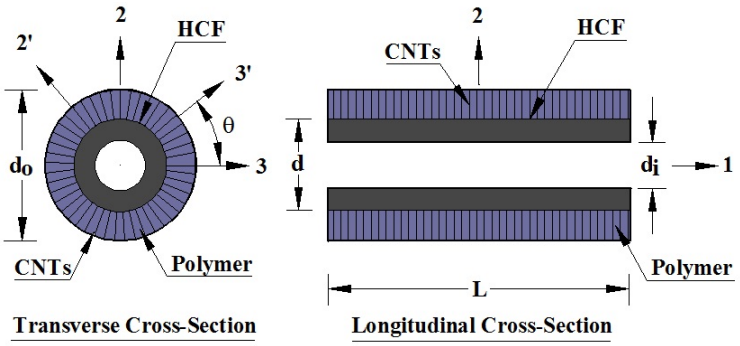

Figure 2. CROSS SECTIONS OF A NOVEL FFHE

THERMAL CONDUCTIVITIES OF A NOVEL FFHE

This Section deals with the procedures of employing two approaches, namely, the method of cells (MOC) approach and the effective medium (EM) approach to predict the effective thermal conductivities of the PMNC material a priori. Subsequently, considering the PMNC material as the matrix phase and the HCF as the reinforcement, the effective thermal conductivities of the FFHE are to be computed. Schematic diagram shown in Fig. 3 demonstrates the various steps involved in the computation of the effective thermal conductivities of the FFHE and are also outlined as follows:

- First, the effective thermal conductivities of the PMNC are to be determined by using either the MOC approach ($R_k = 0$) or the EM approach ($R_k \neq 0$) where R_k is the CNT/polymer matrix interfacial thermal resistance.
- Utilizing the effective orthotropic thermal conductivities of the PMNC material and the isotropic thermal conductivity of the HCF, the effective thermal conductivities of the FFHE can be determined by using the MOC approach.

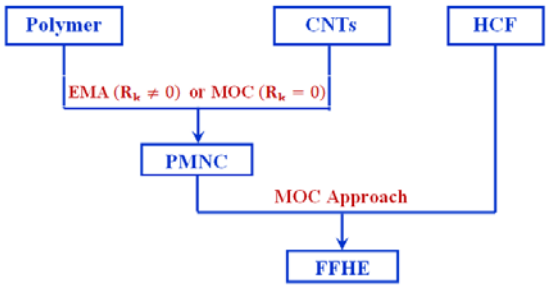

Figure 3. MODELING STEPS OF A NOVEL FFHE

Method of Cells (MOC) Approach: This Section presents the development of the MOC approach to estimate the effective thermal conductivities of the PMNC and the FFHE.

The MOC approach by Aboudi et al. [30] can be modified to predict the effective thermal conductivities of the unwound PMNC material with straight CNTs. From the constructional feature of the FFHE, it may be viewed that the HCF is wrapped by a lamina of the PMNC material. Such an unwound lamina of the PMNC is reinforced by CNTs along its thickness direction (i.e., along the 3–direction) shown in Fig. 4. The average effective thermal conductivities of the PMNC material

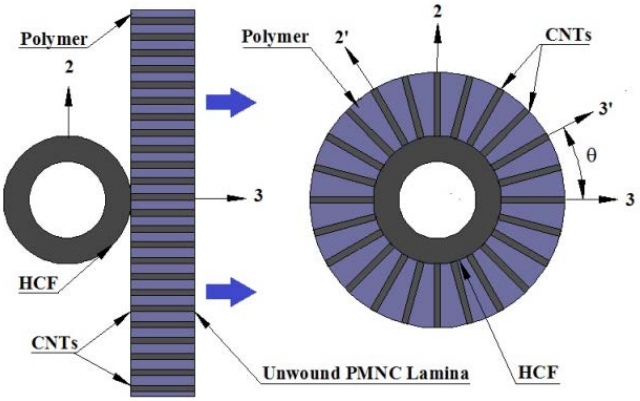

Figure 4. TRANSVERSE CROSS SECTIONS OF A NOVEL FFHE WITH UNWOUND AND WOUND PMNC

surrounding the HCF may be approximated by determining the effective thermal conductivities of this unwound lamina. Thus the analytical procedure for estimating the effective thermal conductivities of the FFHE starts with the estimation of the effective thermal conductivities (K_i^{nc}) of this unwound lamina. Assuming that CNTs are equivalent solid fibers [11, 12, 15–19], uniformly spaced in the polymer matrix and aligned along the 3–axis, the unwound PMNC can be viewed to be composed of cells forming doubly periodic arrays along the x_1– and the x_2–directions. Figure 5 shows a repeating unit cell (RUC) with four subcells. Each rectangular subcell is labeled by β γ, with β and γ denoting the location of the subcell along the x_1– and the x_2–directions, respectively. The subcell can be either a CNT or the matrix. Let four local coordinate systems ($\bar{x}_1^{(\beta)}$, $\bar{x}_2^{(\gamma)}$ and x_3) be introduced, all of which have origins that are located at the centroid of each cell. In accordance with the MOC approach, the deviation of the temperature from a reference temperature T_R (at which the material is stress free when its strain is zero), $\Delta\Theta^{(\beta\gamma)}$, is expanded in the following form:

$$\Delta\Theta^{(\beta\gamma)} = \Delta T + \bar{x}_1^{(\beta)}\xi_1^{(\beta\gamma)} + \bar{x}_2^{(\gamma)}\xi_2^{(\beta\gamma)} \tag{1}$$

where $\xi_1^{(\beta\gamma)}$ and $\xi_2^{(\beta\gamma)}$ characterize the linear dependence of the temperature on the local coordinates.

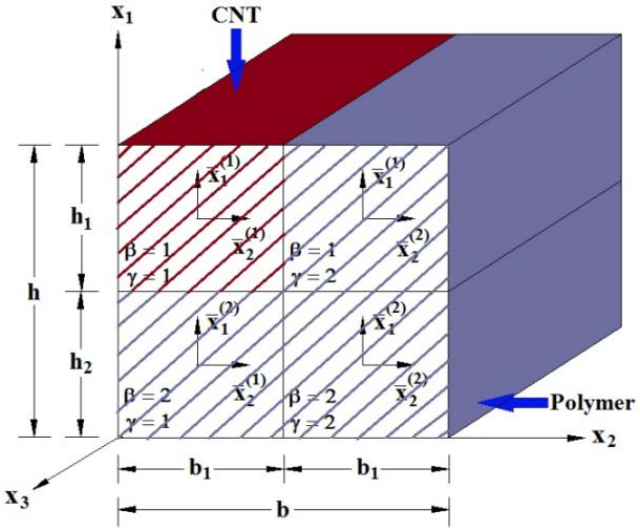

Figure 5. A REPEATING UNIT CELL OF THE PMNC WITH FOUR SUBCELLS (β, γ = 1,2)

The volume ($V_{\beta\gamma}$) of each subcell is

$$V_{\beta\gamma} = b_\beta h_\gamma L \tag{2}$$

where b_β, h_γ and L denote the width, the height and the length of the subcell, respectively, while the area (V) of the RUC is

$$V = bhL \tag{3}$$

The continuity conditions of the temperature at the interfaces of the subcells on an average basis lead to:

$$\begin{aligned} h_1\xi_1^{(1\gamma)} + h_2\xi_1^{(2\gamma)} &= (h_1 + h_2)\frac{\partial T}{\partial x_1} \\ b_1\xi_2^{(\beta 1)} + b_2\xi_2^{(\beta 2)} &= (b_1 + b_2)\frac{\partial T}{\partial x_2} \end{aligned} \tag{4}$$

For the average heat flux in the subcell:

$$\begin{aligned} \bar{q}_1^{(\beta\gamma)} &= -K_1^{(\beta\gamma)}\frac{\partial T}{\partial x_1} \\ \bar{q}_2^{(\beta\gamma)} &= -K_2^{(\beta\gamma)}\frac{\partial T}{\partial x_2} \\ \bar{q}_3^{(\beta\gamma)} &= -K_3^{(\beta\gamma)}\frac{\partial T}{\partial x_3} \end{aligned} \tag{5}$$

where $K_i^{(\beta\gamma)}$ denote the thermal conductivity coefficients of the subcells.

The average heat flux in the unwound PMNC material is determined from:

$$q_i = \frac{1}{V}\sum_{\beta,\gamma=1}^{2} V_{\beta\gamma}\,\bar{q}_i^{(\beta\gamma)} \tag{6}$$

The continuity conditions of the heat flux at the interfaces of the subcells yield

$$\begin{aligned} \bar{q}_1^{(1\gamma)} &= \bar{q}_1^{(2\gamma)} \\ \bar{q}_2^{(\beta 1)} &= \bar{q}_2^{(2\gamma)} \end{aligned} \tag{7}$$

The average heat flux components are related to the temperature gradients by the effective thermal conductivities (K_i^{nc}):

$$\begin{aligned} \bar{q}_1 &= -K_1^{nc}\frac{\partial T}{\partial x_1} \\ \bar{q}_2 &= -K_2^{nc}\frac{\partial T}{\partial x_2} \end{aligned}$$

$$\bar{q}_3 = -K_3^{nc}\frac{\partial T}{\partial x_3} \tag{8}$$

By eliminating the microvariables $\xi_1^{(\beta\gamma)}$ and $\xi_2^{(\beta\gamma)}$, and using the continuity conditions, the effective thermal conductivities of the unidirectional unwound PMNC lamina are given by [30]:

$$K_1^{nc} = \frac{K^p\left\{\begin{matrix}K^n[h(V_{11}+V_{21})+h_2(V_{12}+V_{22})]\\ +K^p h_1(V_{12}+V_{22})\end{matrix}\right\}}{hbL(K^p h_1 + K^n h_2)}$$

$$K_2^{nc} = \frac{K^p\left\{\begin{matrix}K^n[b(V_{11}+V_{12})+b_2(V_{21}+V_{22})]\\ +K^p b_1(V_{21}+V_{22})\end{matrix}\right\}}{hbL(K^p b_1 + K^n b_2)}$$

$$K_3^{nc} = \frac{K^n V_{11} + K^p(V_{12}+V_{21}+V_{22})}{hbL} \tag{9}$$

In Eq. (9), the superscripts nc, n and p represent the unwound PMNC material with straight CNTs, the CNT fiber and the monolithic polymer matrix, respectively; The effective thermal conductivity matrix for the unwound lamina of the PMNC $[K^{nc}]$ can be represented as follows:

$$[K^{nc}] = \begin{bmatrix} K_1^{nc} & 0 & 0 \\ 0 & K_2^{nc} & 0 \\ 0 & 0 & K_3^{nc} \end{bmatrix} \tag{10}$$

It may be noted that the effective thermal conductivity matrix $[K^{nc}]$ directly provides the effective thermal conductivities at a point in the portion of the PMNC material surrounding the HCF where the CNT is aligned with the 3–axis. But for the point located in the PMNC where the CNT is oriented at an angle θ with the 3–axis in the 2–3 plane, $[K^{nc}]$ also provides the effective thermal conductivities with respect to the local material coordinate $(1', 2', 3')$ system. Thus the location dependent effective thermal conductivity matrix $[K^{nc}]$ at any point of the PMNC with respect to the 1–2–3 coordinate system can be obtained by following transformations [31]:

$$[\bar{K}^{PMNC}] = [T]^{-T}[K^{nc}][T]^{-1} \tag{11}$$

in which

$$[T] = \begin{bmatrix} 1 & 0 & 0 \\ 0 & \cos\theta & -\sin\theta \\ 0 & \sin\theta & \cos\theta \end{bmatrix}$$

Therefore, the effective thermal conductivities of the PMNC surrounding the HCF with respect to the principle material coordinate (1, 2, 3) axes of the FFHE vary over an annular cross section of the PMNC phase. A simple homogenization process can be carried out on the RVE of an annular cross section of the PMNC phase to compute its effective properties [31, 32]. Thus without loss of generality, it may be considered that the volume average of these effective thermal conductivities over the volume of the PMNC can be treated as the constant effective thermal conductivities of the PMNC material surrounding the HCF with respect to the 1–2–3 coordinate axes of the FFHE and are given by [32]

$$[K^{PMNC}] = \frac{1}{\pi(R^2-a^2)}\int_0^{2\pi}\int_a^R [\bar{K}^{PMNC}]\, r\, dr\, d\theta \text{ and } \tag{12}$$

It is worthwhile to note that the thermal conductivity matrix of the PMNC $[K^{PMNC}]$ is transversely isotropic. Next, utilizing the transversely isotropic thermal conductivities of the PMNC as the matrix phase and the HCF being aligned along the 1–direction as the reinforcement, the MOC approach can be utilized to compute the effective thermal conductivities (K_i) of the FFHE and are given by:

$$K_1 = \frac{K^f V_{11} + K_1^{PMNC}(V_{12}+V_{21}+V_{22})}{hbL}$$

$$K_2 = \frac{K_2^{PMNC}\left\{\begin{matrix}K^f[h(V_{11}+V_{21})+h_2(V_{12}+V_{22})]\\ +K_2^{PMNC}h_1(V_{12}+V_{22})\end{matrix}\right\}}{hbL\left(K_2^{PMNC}h_1 + K^f h_2\right)}$$

$$K_3 = \frac{K_3^{PMNC}\left\{\begin{matrix}K^f[b(V_{11}+V_{12})+b_2(V_{21}+V_{22})]\\ +K_3^{PMNC}b_1(V_{21}+V_{22})\end{matrix}\right\}}{hbL\left(K_3^{PMNC}b_1 + K^f b_2\right)} \tag{13}$$

Effective Medium (EM) Approach: This Section presents the Maxwell-Garnett type EM approach to estimate the effective thermal conductivities of the PMNC incorporating the CNT/polymer matrix interfacial thermal resistance. Assuming CNTs as solid fibers [11, 12, 15–19], the EM approach by Nan *et al.* [33] can be modified to predict the effective thermal conductivities (K_i^{nc}) of the unwound PMNC material with straight CNT. The effective thermal conductivities of the unwound lamina of the PMNC (K_i^{nc}) are given by [33]

$$K_1^{nc} = K_2^{nc} = K^p\frac{K^n(1+\alpha)+K^p+v_n[K^n(1-\alpha)-K^p]}{K^n(1+\alpha)+K^p-v_n[K^n(1-\alpha)-K^p]}$$

$$K_3^{nc} = v_n K^n + v_p K^p \tag{14}$$

In Eq. (14), a dimensionless parameter $\alpha = 2a_k/d_n$ in which the interfacial thermal property is concentrated on a surface of zero thickness and characterized by Kaptiza radius, $a_k = R_k K^p$; where d_n and R_k represent the diameter of the CNT and the CNT/polymer matrix interfacial thermal resistance, respectively. In Eq. (14), the subscripts v_n and v_p represent the volume fractions of the CNT fiber and the monolithic polymer material, respectively, present in the RVE of the PMNC. Once $[K^{nc}]$ is computed, Eqs. (11) and (12) are used to estimate the average effective thermal conductivities of the PMNC material surrounding the HCF. Next, utilizing the transversely isotropic thermal conductivities of the PMNC as the matrix phase and the HCF being aligned along the 1–direction as the reinforcement, the MOC approach is suitably augmented to compute the effective thermal conductivities of the FFHE.

RESULTS AND DISCUSSION

In this Section, the predictions by the MOC and the EM approaches are first compared with those of the experimental results. Subsequently, the effective thermal conductivities of the FFHE have been determined by utilizing MOC approach in conjunction with the EM approach.

Comparisons with the Experimental Results: The predictions by the MOC and the EM approaches utilized herein are first compared with the experimental results by Marconnet *et al.* [34]. Marconnet *et al.* [34] fabricated the aligned CNT-polymer nanocomposites consisting of multi-walled CNTs arrays infiltrated with an aerospace-grade thermoset epoxy. In their study, the axial and the transverse thermal conductivities of the aligned CNT-polymer nanocomposites are found to be in good agreement against the predictions from the EM approach. For the comparison purpose, the values of thermal conductivities of the multi-walled CNT and the polymer matrix are taken as $K^n = 22.1$ W/mK and $K^p = 0.26$ W/mK, respectively, as considered by Marconnet *et al.* [34]. The comparisons of the axial (K_A) and the transverse (K_T) thermal conductivities of the aligned CNT-polymer nanocomposites estimated by the MOC and the EM

approaches with those of the experimental results [34] are illustrated in Figs. 6 (a) and (b), respectively. In these figures, dotted blue line represents best fits obtained from the EM approach for the experimental results considering an alignment factor (AF) of CNTs as 0.77 observed from the scanning electron microscopy (SEM) [34].

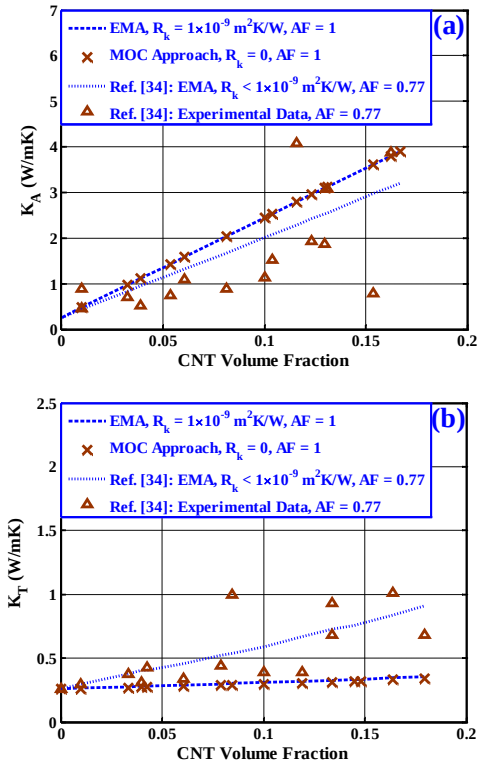

Figure 6. COMPARISONS OF THE EFFECTIVE (a) AXIAL (K_A) AND (b) TRANSVERSE (K_T) THERMAL CONDUCTIVITIES OF THE ALIGNED CNT-POLYMER NANOCOMPOSITE COMPUTED BY THE MOC AND THE EM APPROACHES WITH THOSE OF THE EXPERIMENTAL RESULTS [34]: THE BROWN TRIANGLES REPRESENT THE EXPERIMENTAL DATA FOR THE THERMAL CONDUCTIVITIES; THE DOTTED BLUE LINE REPRESENTS BEST FITS OBTAINED FROM THE EM APPROACH FOR THE EXPERIMENTAL RESULTS CONSIDERING AN ALIGNMENT FACTOR (AF) OF CNTS AS 0.77 OBSERVED FROM THE SEM [34]; THE DASH BLUE LINE AND THE BROWN CROSS SIGNS REPRESENT THE THERMAL CONDUCTIVITIES PREDICTED BY THE EM AND THE MOC APPROACHES, RESPECTIVELY, WHEN THE REINFORCED CNTS ARE PERFECTLY ALIGNED (i.e., AF = 1).

Figure 6 (a) reveal that the axial thermal conductivity (K_A) of the aligned CNT-polymer nanocomposites predicted by the MOC and the EM approaches overestimate the values of K_A by ~21% and ~23% when the values of CNT volume fractions are 0.07 and 0.16, respectively. On the other hand, the MOC and the EM approaches underestimate the values of K_T by 40% and 58% when the values of CNT volume fractions are 0.07 and 0.16, respectively. These differences between the results are attributed to the fact that the perfect alignments of CNTs (i.e., AF = 1) are considered while computing the results by the MOC and the EM approaches whereas the value of AF is 0.77 in Ref. [34]. Possible reasons for the disparity between the analytical and the experimental results include the CNT/matrix interfacial thermal resistance [15-18, 33, 34], lattice defects within CNTs [35, 36], modification of the phonon conduction within CNTs due to interactions with the matrix [37] and the formation of voids in CNT-reinforced composite [38, 39]. In the present study, only the effect of CNT/matrix interfacial thermal resistance on the thermal conductivities of the FFHE is investigated since the CNT/matrix interfacial thermal resistance may significantly affect the thermal conductivities of the PMNC. Investigation of the effect of all other factors is beyond the scope of the present study. It can be inferred from the comparisons shown in Figs. 6 (a) and (b) that the MOC and the EM approaches can be reasonably applied to predict the thermal conductivities of the FFHE.

Analytical Modeling Results: To present the numerical results, the values of thermal conductivities of the armchair (10, 10) CNT and the polymer matrix are considered to be temperature dependence, and the value of thermal conductivity of the HCF is taken as 35.1 W/mK (Torayca-T800H) [40]. The thermal conductivities of the armchair (10, 10) CNT and the polymer are taken as $3.8 \times 10^4 - 3.1 \times 10^3$ W/mK [6] and $0.16 - 0.205$ W/mK [41], respectively, for temperature range $100 - 400$ K. The relationships between the thermal conductivities of the CNT and the polymer with that of the temperature are given by [6, 41]

$$K^n = -2.3476 \times 10^{-18}T^{10} + 5.1847 \times 10^{-15}T^9 - 4.9368 \times 10^{-12}T^8 + 2.6466 \times 10^{-9}T^7 - 8.744 \times 10^{-7}T^6 + 1.8296 \times 10^{-4}T^5 - 0.02398T^4 + 1.8888T^3 - 85.366T^2 + 2256.4T \ \text{W/mK} \quad (14)$$

$$K^p = -1.2805 \times 10^{-15}T^6 + 1.8231 \times 10^{-12}T^5 - 1.0343 \times 10^{-9}T^4 + 2.9748 \times 10^{-7}T^3 - 4.6272 \times 10^{-5}T^2 - 0.0040278T \ \text{W/mK} \quad (15)$$

The values of inner (d_i) and outer (d_o) diameters of the bare HCF (without CNTs) heat exchanger and the FFHE are kept constant to 50 μm and 100 μm, respectively. The determination of the CNT volume fraction in the FFHE is an important issue. It is obvious that the constructional feature of the FFHE imposes a constraint on the maximum value of the CNT volume fraction. The maximum CNT volume fraction in the FFHE can be determined based on the surface to surface distance at the roots of the two adjacent CNTs as 1.7 nm [28], the CNT diameter (d_n) and the outer diameter of the HCF (d) in the FFHE as follows:

Referring to Fig. 2, the volumes of the HCF (V^F), the PMNC (V^{PMNC}) and the FFHE (V^{FFHE}) are given by

$$V^F = \frac{\pi}{4}(d^2 - d_i^2)L \quad (16)$$

$$V^{PMNC} = \frac{\pi}{4}(d_o^2 - d^2)L \quad (17)$$

$$V^{FFHE} = \frac{\pi}{4}(d_o^2 - d_i^2)L \quad (18)$$

Using Eqs. (16) and (18), the volume fraction of the HCF (v_f) in the FFHE can be determined as

$$v_f = \frac{V^F}{V^{FFHE}} = \frac{(d^2 - d_i^2)}{(d_o^2 - d_i^2)} \quad (19)$$

The maximum number of radially grown aligned CNTs $(N_{CNT})_{max}$ on the outer circumferential surface of the HCF is given by

$$(N_{CNT})_{max} = \frac{\pi dL}{(d_n + 1.7)^2} \quad (20)$$

Therefore, the volume of the CNTs (V^{CNT}) is

$$V^{CNT} = \frac{\pi}{8}d_n^2(d_o - d)(N_{CNT})_{max} \quad (21)$$

Thus the maximum volume fraction of the CNTs $(V_{CNT})_{max}$ with respect to the volume of the FFHE can be determined as

$$(V_{CNT})_{max} = \frac{V^{CNT}}{V^{FFHE}} = \frac{d_n^2(d_o - d)}{2(d_o^2 - d_i^2)L}(N_{CNT})_{max} \quad (22)$$

The maximum volume fraction of the CNTs with respect to the volume of the PMNC $(v_n)_{max}$ can be determined in terms of $(V_{CNT})_{max}$ as follows:

$$(v_n)_{max} = \frac{V^{CNT}}{V^{PMNC}} = \frac{(d_o^2 - d_i^2)}{(d_o^2 - d^2)}(V_{CNT})_{max} \quad (23)$$

First, the effective thermal conductivities of the PMNC material surrounding the HCF are computed by utilizing the models presented in previous Section. Unless otherwise mentioned, the effective thermal conductivities of the PMNC are computed considering the perfect CNT/polymer matrix interface without any interfacial thermal resistance (i.e., $R_K = 0$). It should be noted that the value of CNT volume fraction in the PMNC varies with the variation of the HCF volume fraction in the FFHE. The CNT volume fraction in the PMNC $(v_n)_{max}$ given by Eq. (23) has been used to determine the effective thermal conductivities of the PMNC. Figures 7 (a) and (b) illustrate the variation of the axial (K_1^{PMNC}) and the transverse (K_2^{PMNC}) thermal conductivities of the PMNC, respectively, with the CNT volume fraction in the PMNC when the value of d is 60 µm. Maximum value of $(v_n)_{max}$ in

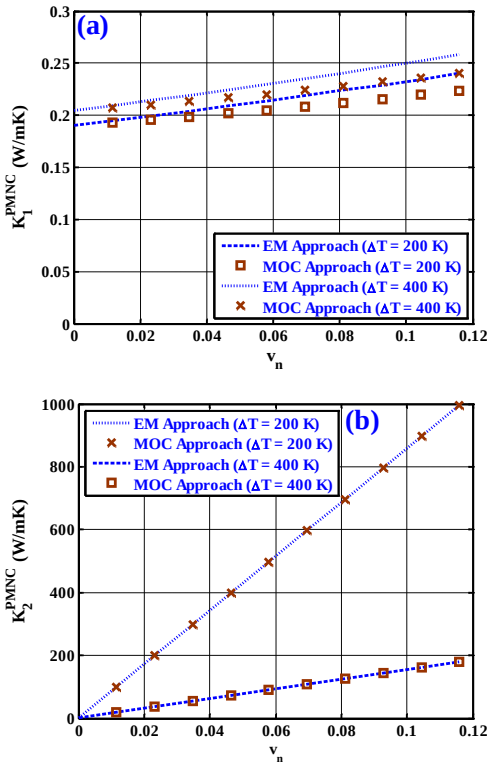

Figure 7. VARIATIONS OF THE EFFECTIVE (a) AXIAL (K_1^{PMNC}) AND (b) TRANSVERSE (K_2^{PMNC}) THERMAL CONDUCTIVITIES OF THE PMNC WITH THE CNT VOLUME FRACTION IN THE PMNC ($R_k = 0$).

the PMNC reaches up to 0.1164 when the value of diameter of the HCF (d) is 60 µm. It may be observed from these figures that the effective values of K_1^{PMNC} and K_2^{PMNC} are enhanced with the increase in the value of CNT volume fraction in the PMNC. These figures also reveal that the thermal conductivities predicted by the EM approach agree with those predicted by the MOC approach for both the values of temperature. This is attributed to the fact that CNTs are considered to be perfectly aligned in the PMNC (i.e., AF = 1) and the value of CNT/polymer matrix interfacial thermal resistance is considered as zero ($R_k = 0$). Since the PMNC is transversely isotropic with the 1– axis as the axis of symmetry, the effective values of K_3^{PMNC} of the PMNC are found to be identical to those of K_2^{PMNC} and hence are not presented here. Since the effective thermal conductivities of the PMNC predicted by the EM approach and the MOC approach are transversely isotropic, the MOC approach is utilized to estimate the effective thermal conductivities of the FFHE.

The effect of radial growing of CNTs on the circumferential surface of the HCF has been studied by considering the values of d = 60 µm, T = 200 K and T = 400 K. However, the variations of the CNT volume fraction in the FFHE and the temperature for a particular value of d would be an important study. For this the discrete values of d are considered as 60 µm, 70 µm, 80 µm and 90 µm. Figures 8 (a) and (b) illustrate the variations of the axial (K_1) and the transverse (K_2) thermal conductivities of the FFHE with the temperature. It may be observed from Fig. 8 (a) that the radial

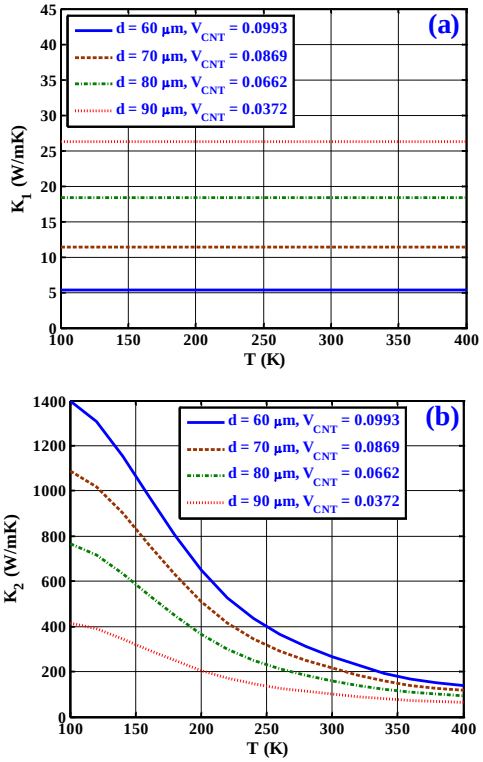

Figure 8. VARIATIONS OF THE EFFECTIVE (a) AXIAL (K_1) AND (b) TRANSVERSE (K_2) THERMAL CONDUCTIVITIES OF THE FFHE WITH THE TEMPERATURE ($R_k = 0$).

growing of CNTs on the HCF does not influence the value of K_1 of the FFHE in the axial direction. On the other hand, Fig. 8 (b) reveal that the value of K_2 decreases with the increase in the temperature. This is attributed to the fact that the thermal conductivity (K^n) of the radially grown CNTs on the circumferential surface of the HCF significantly decreases with the increase in the temperature which eventually lowers the effective value of K_2 of the PMNC. It may also be importantly observed from Fig. 8 (b) that when the value of d is 60 µm and corresponding value of the CNT volume fraction in the FFHE is 9.93%, almost 661% and 293% enhancements occurred in the values of K_2 of the FFHE over those of the bare HCF (i.e., without CNTs) heat exchanger, respectively, if the values of temperature are 300 K and 400 K. This is attributed to the fact that the radially grown CNTs enhance the out-of-plane thermal conductivities of the PMNC surrounding the HCF. Although not presented here, the computed effective values of K_3 are found to match identically with those of K_2 corroborating the fact that the FFHE is transversely isotropic

about the 1-axis.

So far the effect of CNT/polymer matrix interfacial thermal resistance on the effective thermal conductivities of the PMNC has been neglected. However, the CNT/polymer matrix interfacial thermal resistance may affect the thermal conductivities of the PMNC and consequently, degrade the performance of the FFHE. Hence, to analyze the effect of CNT/polymer matrix interfacial thermal resistance on the effective thermal conductivities of the FFHE, the value of R_k is varied up to 20×10^{-8} m^2K/W [13, 14]. Figure 9 illustrates the variation of the effective thermal conductivity K_1^{PMNC} of the PMNC incorporating the CNT/polymer matrix interfacial thermal resistance when the value of T = 400 K. It may be observed from this figure that the value of K_1^{PMNC} decreases rapidly with the increase in the value of R_k up to 3×10^{-8} m^2K/W and beyond a value of $R_k = 3 \times 10^{-8}$ m^2K/W, the value of K_1^{PMNC} stabilizes. Although not presented here, the values of K_2^{PMNC}, K_3^{PMNC}, K_1, K_2 and K_3 are found to be independent of the values of R_k.

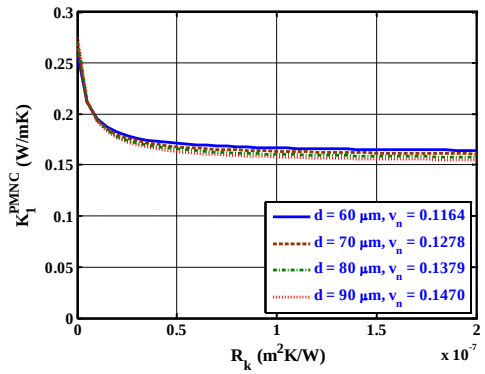

Figure 9. VARIATION OF THE EFFECTIVE AXIAL THERMAL CONDUCTIVITY (K_1^{PMNC}) OF THE PMNC WITH THE CNT/POLYMER INTERFACIAL THERMAL RESISTANCE (T = 400 K).

CONCLUSIONS

A novel fuzzy carbon fiber heat exchanger (FFHE) is proposed in this study which is comprised of the CNTs, the polymer matrix and the hollow cylindrical carbon fiber (HCF). Thermal conductivities of a novel FFHE have been estimated by employing the MOC approach in conjunction with the EM approach. The following main conclusions are drawn from the present study:

1. Since the CNTs are radially grown on the circumferential surface of the HCF, the effective transverse thermal conductivities of the FFHE are significantly improved over those of the bare HCF (i.e., without CNTs) heat exchanger. On the other hand, the effective axial thermal conductivity of the FFHE slightly decreased when the CNTs are present on the circumferential surface of the HCF.
2. The CNT/polymer matrix interfacial thermal resistance does not affect the effective thermal conductivities of the FFHE.

Since the transverse thermal conductivities of the FFHE are significantly enhanced, the FFHE will have better heat transfer performance compared to that of the bare HCF heat exchanger. Such novel FFHE can be properly used as heat exchangers those require stringent constraint on the dimensional stability with better heat transfer characteristics for developing light weight and high strength heat exchangers in advanced technological applications. The present analysis may also motivate the researchers for constructing a novel heat exchanger and serve the purpose of verifying the experimental estimates.

REFERENCES

[1] Iijima, S., 1991. "Helical Microtubules of Graphitic Carbon". *Nature*, **354**, November, pp. 56–58.

[2] Treacy, M.M.J., Ebbesen, T.W., and Gibson, J.M., 1996. "Exceptionally High Young's Modulus Observed for Individual Carbon Nanotubes". *Nature*, **381**, June, pp. 678–680.

[3] Li, C., and Chou, T.W., 2003. "A Structural Mechanics Approach for the Analysis of Carbon Nanotubes". *International Journal of Solids of Structures*, **40**(10), May, pp. 2487–2499.

[4] Shen, L., and Li, J., 2004. "Transversely Isotropic Elastic Properties of Single-walled Carbon Nanotubes". *Physical Review B*, **69**(4), January, p. 045414.

[5] Hone, J., Whitney, M., Piskoti, C., and Zettl, A., 1999. "Thermal Conductivity of Single-walled Carbon Nanotubes". *Physical Review B*, **59**(4), January, pp. 2514–2516.

[6] Berber, S., Kwon, Y.K., and Tomanek, D., 2000. "Unusually High Thermal Conductivity of Carbon Nanotubes". *Physical Review Letters*, **84**(20), May, pp. 4613–4616.

[7] Lukes, J.R., and Zhong, H., 2007. "Thermal Conductivity of Individual Single-Wall Carbon Nanotubes". *ASME Journal of Heat Transfer*, **129**, June, pp. 705–116.

[8] Wei, L., Yanhui, F., Jia, P., and Xinxin, Z., 2012. "Effects of Stone-Wales Defects on the Thermal Conductivity of Carbon Nanotubes". *ASME Journal of Heat Transfer*, **134**, September, p. 092401.

[9] Choi, S.U.S., Zhang, Z.G., Lockwood, F.E., and Grulke, E.A., 2001. "Anomalous Thermal Conductivity Enhancement in Nanotube Suspensions". *Applied Physics Letters*, **79**(14), October, pp. 2252–2254.

[10] Biercuk, M.J., Llaguno, M.C., Radosavljevic, M., Hyun, J.K., and Johnson, A.T., 2002. "Carbon Nanotube Composites for Thermal Management". *Applied Physics Letters*, **80**(15), April, pp. 2767–2769.

[11] Guthy, C., Du, F., Brand, S., Winey, K.I., and Fischer, J.E., 2007. "Thermal Conductivity of Single-Walled Carbon Nanotube/PMMA Nanocomposites". *ASME Journal of Heat Transfer*, **129**, August, pp. 1096–1099.

[12] Nan, C.W., Shi, Z., and Lin, Y., 2003. "A Simple Model for Thermal Conductivity of Carbon Nanotube-Based Composites". *Chemical Physics Letters*, **375**, July, pp. 666–669.

[13] Wilson, O.M., Hu, X., Cahill, D.G., and Braun, P.V., 2002. "Colloidal Metal Particles as Probes of Nanoscale Thermal Transport in Fluids". *Physical Review B*, **66**(22), December, p. 224301.

[14] Huxtable, S.T., Cahill, D.G., Shenogin, S., Xue, L., Ozisik, R., Barone, P., Usrey, M., Strano, M.S., Siddons, G., Shim, M., and Keblinski, P., 2003. "Interfacial Heat Flow in Carbon Nanotube Suspensions". *Nature Materials*, **2**(11), October, pp. 731–734.

[15] Nan, C.W., Liu, G., Lin, Y., and Lin, M., 2004. "Interface Effect on Thermal Conductivity of Carbon

Nanotube Composites". *Applied Physics Letters*, **86**(16), October, pp. 3549–3551.
[16] Bryning, M.B., Milkie, D.E., Islam, M.F., Kikkawa, J.M., and Yodh, A.G., 2005. "Thermal Conductivity and Interfacial Resistance in Single-Wall Carbon Nanotube Epoxy Composites". *Applied Physics Letters*, **87**, October, p. 161909.
[17] Xue, Q.Z., 2006. "Model for the Effective Thermal Conductivity of Carbon Nanotube Composites". *Nanotechnology*, **17**(6), February, pp. 1655–1660.
[18] Cherkasova, A.S., and Shan, J.W., 2010. "Particle Aspect-Ratio and Agglomeration-State Effects on the Effective Thermal Conductivity of Aqueous Suspensions of Multiwalled Carbon Nanotubes". *ASME Journal of Heat Transfer*, **132**, August, p. 082402.
[19] Maruyama, S., and Xiang, R., 2012. "Chemical Vapor Deposition Growth, Optical, and Thermal Characterization of Vertically Aligned Single-Walled Carbon Nanotubes". *ASME Journal of Heat Transfer*, **134**, May, p. 051024.
[20] Bower, C., Zhu, W., Jin, S., and Zhou, O., 2000. "Plasma-Induced Alignment of Carbon Nanotubes". *Applied Physics Letters*, **77**(6), August, pp. 830–832.
[21] Thostenson, E.T., Li, W.Z., Wang, D.Z., and Chou, T.W., 2002. "Carbon Nanotube/Carbon Fiber Hybrid Multiscale Composites". *Applied Physics Letters*, **91**(9), May, pp. 6034–6037.
[22] Zhao, Z.G., Ci, L.J., Cheng, H.M., and Bai, J.B., 2005. "The Growth of Multi-walled Carbon Nanotubes with Different Morphologies on Carbon Fibers". *Carbon*, **43**, November, pp. 651–673.
[23] Veedu, V.P., Cao, A., Li, X., Ma, K, Soldano, C., Kar, S., Ajayan, P.M., and Ghasemi-Nejhad, M.N., 2006. "Multifunctional Composites Using Reinforced Laminae with Carbon-Nanotube Forests". *Nature Materials*, **5**, June, pp. 457–462.
[24] Bekyarova, E., Thostenson, E.T., Yu, A., Kim, H, Gao, J., Tang, J., Hahn, H.T., Chou, T.W., Itkis, M.E., and Haddon, R.C., 2007. "Multiscale Carbon Nanotube-Carbon Fiber Reinforcement for Advanced Epoxy Composites". *Langmuir*, **23**(7), February, pp. 3970–3974.
[25] Yamamoto, N., Wicks, S.S., Guzman de Villoria, R., Ishiguro, K., Steiner III, S.A., Garcia, E.J., and Wardle, B.L., 2009. "Mechanical, Thermal, and Electrical Properties of Woven Laminated Advanced Composites Containing Aligned Carbon Nanotubes". *17th International Conference on Composite Materials*, Edinburgh, Scotland, July 27–31.
[26] Chen, J., Xiong, X., and Xiao, P., 2009. "The Effect of Carbon Nanotube Growing on Carbon Fibers on the Microstructure of the Pyrolytic Carbon and the Thermal Conductivity of Carbon/Carbon Composites". *Materials and Chemistry Physics*, **116**(1), July, pp. 57–61.
[27] Yamamoto, N., de Villoria, R.G., Cebeci, H.G., and Wardle, B. L., 2010. "Thermal and Electrical Transport in Hybrid Woven Composites Reinforced with Aligned Carbon Nanotubes". *Proceedings of 51st AIAA Structures, Structural Dynamics and Materials Conference*, Orlando, FL, April 12–15.
[28] Kundalwal, S.I., and Ray, M.C., 2011. "Micromechanics Analysis of Fuzzy Fiber Reinforced Composites". *International Journal of Mechanics and Materials in Design*, **7**(2), June, pp. 149–166.
[29] Chatzigeorgiou, G., Seidel, G. D., and Lagoudas, D. C., 2012. "Effective Mechanical Properties of "Fuzzy Fiber" Composites". *Composites Part B*, **43**(6), September, pp. 2577–2593.
[30] Aboudi, J., Arnold, S.M., Bednarcyk, B.A., 2012. *Micromechanics of Composite Materials: A Generalized Multiscale Analysis Approach*. Butterworth-Heinemann Ltd, Oxford OX5, UK.
[31] Hatta, H., and Taya, M., 1985. "Effective Thermal Conductivity of a Misoriented Short Fiber Composite". *Journal of Applied Physics*, **58**(7), October, pp. 2478–2486.
[32] Cowin, S.C., and Fraldi, M., 2005. "On Singularities Associated with the Curvilinear Anisotropic Elastic Symmetries". *International Journal of Nonlinear Mechanics*, **40**, March-April, pp. 361–371.
[33] Nan, C.W., Birringer, R., Clarke, D.R., and Gleiter, H., 1997. "Effective Thermal Conductivity of Particulate Composites with Interfacial Thermal Resistance". *Journal of Applied Physics*, **81**(10), May, pp. 6692–6699.
[34] Marconnet, A.M., Yamamoto, N., Panzer, M.A., Wardle, B.L., and Goodson, K.E., 2011. "Thermal Conduction in Aligned Carbon Nanotube-Polymer Nanocomposites with High Packing Density" . *ACS Nano*, **5**(6), May, pp. 4841–4825.
[35] Yu, A., Itkis, M.E., Bekyarova, E., and Haddon, R.C., 2006. "Effect of Single-Walled Carbon Nanotube Purity on the Thermal Conductivity of Carbon Nanotube-Based Composites". *Applied Physics Letters*, **89**, September, p. 133102.
[36] Ivanov, I., Puretzky, A., Eres, G., Wang, H., Pan, Z., Cui, H., Jin, R., Howe, J., and Geohegan, D.B., 2006. "Fast and Highly Anisotropic Thermal Transport Through Vertically Aligned Carbon Nanotube Arrays". *Applied Physics Letters*, **89**, November, p. 223110.
[37] Gojny, F.H., Wichmann, M.H.G., Fiedler, B., Kinloch, I.A., Bauhofer, W., Windle, A.H., and Schulte, K., 2006. "Evaluations and Identification of Electrical and Thermal Conduction Mechanisms in Carbon Nanotubes/Epoxy Composites". *Polymer*, **47**(6), March, pp. 2036–2045.
[38] Grunlan, J.C., Kim, Y.S., Ziaee, S., Wei, X., Abdel-Magid, B., and Tao, K., 2006. "Thermal and Mechanical Behavior of Carbon-Nanotube-Filled Latex". *Macromolecular Material Engineering*, **291**(9), September, pp. 1035–1043.
[39] Borca-Tasciuc, T., Mazumdar, M., Son, Y., Pal, S.K., Schadler, L.S., and Ajayan, P.M., 2007. "Anisotropic Thermal Diffusivity Characterization of Aligned-carbon Nanotube-Polymer Composites". *Journal of Nanoscience and Nanotechnology*, **7**, April-May, pp. 1581–1588.
[40] TORAYCA. *Technical Data Sheet No. CFA-007*, Toray Carbon Fibers America, Inc., 6 Hutton Centre Drive, Santa Ana, CA. See also URL http://www.toraycfa.com/pdfs/T800HDataSheet.pdf
[41] Reese, W., 1996. "Low-Temperature Thermal Conductivity of Amorphous Polymers: Polystyrene and Polymethylmethacrylate". *Journal of Applied Physics*, **37**(2), February, pp. 864–868.